Observability of Ionospheric Space-Time Structure with ISR: A simulation study

John Swoboda,[1] Joshua Semeter,[1] Philip Erickson[2]

———

[1]Department of Electrical & Computer Engineering, Boston University, Boston, Massachusetts, USA.

[2]Haystack Observatory, Massachusetts Institute of Technology, Westford, Massachusetts, USA.

As with any sensing modality incoherent scatter radar (ISR) has inherent errors and uncertainty in its measurements. A number of theoretical aspects behind these errors have been documented in the literature, which leads to a trade off between spatial and temporal resolution and statistical accuracy.

Resource allocation and experiment design. Understand degrees of freedom in design.

The recent application of phased array antennas with pulse to pulse steering allow for greater flexibility in processing along with making it is now possible to create full volumetric reconstructions of plasma parameters. These phased array systems are used heavily in the high latitude region of the ionosphere, which can have plasma phenomena that is highly variable in space and time. In order to develop an experiment to observe the plasma phenomena researchers have to wade through a large number of degrees of freedom. In order to properly allocate resources in some cases researchers may need to simulate the experiment.

This publication will show a simulator that can take a field of plasma parameters and create ISR data at the IQ level and then process it to show a possible reconstruction of the parameters field. This simulator can be used to create ISR data to test new algorithms to better reconstruct the plasma parameter field. It can also give researchers a new tool that can assist them

24 in the set up their experiments. This simulation will overall give a full for-

25 ward model description of the ISR reconstruction.

1. Introduction

Incoherent scatter radar is an important diagnostic for the ionosphere in that it can give direct measurements of the intrinsic plasma parameters [*Dougherty and Farley*, 1960; *Farley et al.*, 1961; *Dougherty and Farley*, 1963; *Hagfors*, 1961]. As with all diagnostic tools it has associated with it sources of errors which include time and spatial ambiguities [*Farley*, 1969a, b; *Hysell et al.*, 2008; *Swoboda et al.*, 2015].

One unique aspect of ISR is that inherent random fluctuations of the plasma are used to create these measurements. These fluctuations are used by creating second order statistics from a scattered signal, specifically an autocorrelation function (ACF) [*Farley*, 1969a]. The statistical nature of the target itself yields the requirement of averaging numerous realizations of the ACF to reduce the variance of the estimate. This forces the assumption of stationarity for a space-time cell, which may not be true. In the end this creates a trade-off between space-time resolution and the variance of the measurements.

Application of electronically steerable array (ESA) technology to ISR has been a recent advancement for the community. ISRs such as these, like the Advanced Modular Incoherent Scatter (AMISR) systems, have already been deployed in Poker Flat Alaska and Resolute Bay Canada [*Nicolls and Heinselman*, 2007; *Dahlgren et al.*, 2012a]. These ESA based systems are seen as the future of the ISR sensor modality due to the flexibility in beam steering, processing and other aspects over dish based systems. The next step in the evolution of these systems is expected to be the EISCAT-3D project, which will have a number of enhancements such as multi-static

47 processing capability and be able to receive and process data from each phased array

48 element by default.

49 One benefit of ESA based ISR is that volumetric reconstructions of plasma param-

50 eters can be created [*Semeter et al.*, 2009; *Nicolls and Heinselman*, 2007; *Dahlgren*

51 *et al.*, 2012a]. These systems also have ben used to reconstuct full vector parameters

52 using estimates of the ion velocity which can be determined using the Doppler shift

53 of spectra [*Butler et al.*, 2010; *Nicolls et al.*, 2014]. Still it has been shown that the

54 volumetric reconstructions can yield measurements with a high degree of ambiguity

55 [*Dahlgren et al.*, 2012b].

56 Due to this

2. Space-Time Errors

3. Simulator

57 The goal of incoherent scatter radar is to measure plasma parameters by first

58 estimating a power spectrum from the random fluctuations of the electron density

59 in the ionosphere. In order to model the the return signal from an ISR a complex

60 gaussian process with a correlation properties dictated by the plasma parameters is

61 created. In this chapter the methods used to create the ISR data are detailed. The

62 First the inputs will be covered, after which the signal processing procedures to make

63 the base band IQ data will be shown.

3.1. Inputs

The simulator takes as input a discretized set of ionosphere parameters in Cartesian coordinates and which can change with time. Each point in time and space has a set of parameters that allow it to make an ISR spectrum using the methods detailed in the previous chapter. The spectrums are then created so every point in space and time will have its own intrinsic ISR spectrum. The radar will then act on these spectrums as a linear operator and average them together in time and space using the beam patterns and pulse pattern.

Using the fact that any spatial correlations between the electron density fluctuations will be on the order of the Debye length *Farley* [1969a], the intrinsic ISR spectrums will be first averaged over a resolution cell for the radar.

3.2. Signal Processing

The IQ data is created by taking a complex white Gaussian noise process and shaping the spectrum using a filter. Each point in space and time will have a separate noise plant and filter which is derived from the plasma and radar parameters parameters, like that seen in Figure 1.

The radar samples the space in a spherical coordinate system with discrete range and beam positions. For each range gate and beam the different spectrums are averaged together together. In range this is simply a window the length of a range gate. Across the azimuth and elevation space the beam pattern for the system is used. In order to calculate the beam pattern for the AMISR system the method

detailed in the appendix of [*Swoboda et al.*, 2015]. The entire process of the spatial

sample is shown in the simplified diagram in Figure 2.

Once the spectrum has been created the filter, $H_m(\omega)$, is created by simply taking

the square root of the spectrum, $S_m(\omega|\,\boldsymbol{\theta})$

$$H_m(\omega) = \sqrt{S_m(\omega|\,\boldsymbol{\theta})}. \tag{1}$$

The term $\boldsymbol{\theta}$ refers to the different plasma and system parameters needed to make the

spectrum. Complex white Gaussian noise, CWGN, $(w(k) \sim CN(0, \mathbf{I}))$ is then pushed

though each of the filters and then windowed by the pulse creating the following:

$$y_m(k) = s(k)\left[h_m(k) * w(k)\right], \tag{2}$$

where $s(k)$ is the pulse shape. The application of this filter is actually done in the

frequency domain. This is possible because the Discrete Fourier Transform (DFT)

of a vector of CWGN is also CWGN. The only difference is that there is a change

in the variance, which is tied to the number of points used in the DFT [*Kay*, 1993].

With this in mind Equation 2 can be implemented as the following,

$$y_m(k) = s(k) \sum_{i=0}^{K-1} e^{j\omega_i k} \left[\sqrt{S_m(\omega_i|\,\boldsymbol{\theta})} w(\omega_i)\right], \tag{3}$$

where ω_i is the frequency variable, $w(\omega_i) \sim CN(0, \mathbf{I})$ and K is the number of points

used for the DFT [*Mitchell and Mcpherson*, 1981].

After the data for each range gate $y_m(k)$ is created the power of the return is
calculated

$$P_r = \frac{cG\lambda^2}{2(4\pi)^2} \frac{P_t}{R^2} \frac{\sigma_e N_e}{(1 + k^2\lambda_D^2),(1 + k^2\lambda_D^2 + T_r)} \tag{4}$$

where P_r is the power received, c is the speed of light, G is the gain of the antenna,
P_t is the power of the transmitter, σ_e is the electron radar cross section, k is the
wavenumber of the radar, λ_D is the Debye length, N_e is the electron density and T_r
is the electron to ion temperature ratio.

Once the power has been calculated for each range all of the data is delayed and
summed together so as to model the arrival of the radar return at the receive:

$$x(n) = \sum_{m=0}^{M-1} \alpha(m)y_m(n-m), \tag{5}$$

where $\alpha(m) = \sqrt{P_r(m)}/\hat{\sigma}_y$ and $\hat{\sigma}_y$ is the estimate of the standard deviation of $y_m(k)$.
Lastly, to model the inherent noise in the radar and environment more complex
Gaussian noise is added

$$x_f(n) = x(n) + \sqrt{\frac{k_b T_{sys} B}{2}} w(n), \quad w(n) \sim CN(0,1) \tag{6}$$

where k_b is Boltzmann's constant, T_{sys} is the system temperature and B is the system
bandwidth. A full diagram of the model can be seen in Figure 3.

3.3. ISR Processing

After the IQ data has been created it is processed to create estimates of the ACF at desired points of space. This type of processing has been detailed and analyzed in [*Farley*, 1969a] and in other publications. This processing follows a flow chart seen in Figure 4.

3.4. Lag Product Formation

The lag product formation is an initial estimate of the autocorrelation function. The sampled I/Q can be represented as $x(n) \in \mathbb{C}^N$ where N is the number of samples in an inter pulse period. For each range gate $m \in 0, 1, ...M - 1$ an autocorrelation is estimated for each lag of $l \in 0, 1..., L - 1$. To get better statistics this operation is performed for each pulse $j \in 0, 1, ...J - 1$ and then summed over the J pulses. The entire operation to form the initial estimate of $\hat{R}(m, l)$ can be seen in Equation 9:

$$\hat{R}(m, l) = \sum_{j=0}^{J-1} x(m - \lfloor l/2 \rfloor, j)x^*(m + \lceil l/2 \rceil, j). \qquad (7)$$

The case shown in Equation 9 is a centered lag product, other types of lag products calculations are available but generally a centered product is used. In the centered lag product case range gate index m and sample index n can be related by $m = n - \lfloor L/2 \rfloor$ and the maximum lag and sample relation is $M = N - \lceil L/2 \rceil$. This lag product formation is the first step in taking a discrete Wigner Distribution [*Cohen*, 1995].

This specific type of lag product formation is detailed in [*Farley*, 1969a] and had been referred to as unbiased. This terminology does differ from what is used in

₁₂₇ statistic signal processing literature such as [*Shanmugan and Breipohl*, 1988] where

₁₂₈ the unbiased autocorrelation function estimate is carried out as so,

$$\hat{R}(m,l) = \frac{1}{L-l} \sum_{j=0}^{J-1} x(m - \lfloor l/2 \rfloor, j) x^*(m + \lceil l/2 \rceil, j). \qquad (8)$$

₁₂₉ With out the $\frac{1}{L-l}$ term the estimator will be windowed with a triangular function

₁₃₀ thus impacting the estimate of the ISR spectrum as this will act as a convolution in

₁₃₁ the frequency domain. This bias is taken into account in [*Farley*, 1969a] but it is

₁₃₂ simply wrapped up into the ambiguity function.

3.5. Summation Rules

₁₃₃   Applying a summation rule is usually the next step in creating an estimate of the

₁₃₄ autocorrelation function. This is done to get a constant range ambiguity across all

₁₃₅ of the lags for long pulse experiment[*Nygren*, 1996]. It also equalizes the statistics

₁₃₆ for each lag as the higher lags have greater variance.

₁₃₇   An example summation rule for a forward product is shown in Figure 5. In the

₁₃₈ figure the image on the left is a basic representation of an ambiguity function of a

₁₃₉ long pulse. Its mirrored on the right with red bars which would show the integration

₁₄₀ area under it so the ambiguity function will be of equal size in range.

₁₄₁   In the processing this is basically a summing of lags from different ranges. The

₁₄₂ amount of summing is similar to what is shown in Figure 5. There are a number of

₁₄₃ different summing rule each with their own trade offs [*Nygren*, 1996].

₁₄₄   Lastly an estimate of the noise correlation is subtracted out of $\hat{R}(m,l)$, which is

₁₄₅ defined as $\hat{R}_w(m,l)$:

$$\hat{R}_w(m,l) = \sum_{j=0}^{J-1} w(m_w - \lfloor l/2 \rfloor, j) w^*(m_w + \lceil l/2 \rceil, j), \tag{9}$$

where $w(n_w)$ is the background noise process of the radar. Often the noise process

is sampled during a calibration period for the radar when nothing is being emitted.

The final estimate of the autocorrelation function after the noise subtraction and

summation rule will be represented by $\hat{R}_f(m,l)$.

3.6. Nonlinear Least-Squares Fitting

After the final estimation of the spectrum is complete the nonlinear least squares

fitting takes place to determine the parameters. The basic class of nonlinear least-

squares problems as seen in [*Kay*, 1993], are shown in Equation 10,

$$\hat{\mathbf{p}} = \underset{\mathbf{p}}{\operatorname{argmin}} (\mathbf{y} - \boldsymbol{\theta}(\mathbf{p}))^* \boldsymbol{\Sigma}^{-1} (\mathbf{y} - \boldsymbol{\theta}(\mathbf{p})). \tag{10}$$

In Equation 10, the data represented as $\mathbf{y}$ would be the final estimate of the au-

tocorrelation function $\hat{R}_f(m,l)$ at a specific range or its spectrum $\hat{S}_f(m,\omega)$. The

parameter vector $\mathbf{P}$ would be the plasma parameters N_e, T_e, T_i and various other

parameters including ion velocities. The fit function $\boldsymbol{\theta}$ is the IS spectrum calculated

from models, such as once seen in [*Kudeki and Milla*, 2011], smeared by the ambi-

guity function. In the case of the long pulse the ambiguity can be simply applied

by multiplying it with the autocorrelation function $R(l)$, if the summation rule is

properly applied. The correlation matrix $\boldsymbol{\Sigma}$ is often realized as a diagonal matrix for

161 many ISR systems the variance of the lags or each point of the spectrum being the

162 values. The variance of the ACF estimator can be estimated using the following,

$$\sigma^2_{\hat{R}(l)} = \frac{1}{JL} \sum_{m=-(L-l-1)}^{L-l-1} \left(\frac{L - |m| + 1}{L}\right) \left(|\hat{R}(m)|^2 + |\hat{R}(m+l)\hat{R}(m-l)|\right) + \hat{N}^2 \quad (11)$$

163 where N is the estimated noise power. To estimate the spectrum variance the matrix

164 $\mathbf{\Sigma}$ is transformed in to the Fourier domain using FFTs (FFT on the columns and

165 IFFT on the rows) so as to model the $\mathbf{F\Sigma F}^*$ matrix operation.

166   In the past ISR researchers have used the Levenberg-Marquart algorithm to fit

167 data [*Nikoukar et al.*, 2008]. This specific iterative algorithm moves the parameter

168 vector $\mathbf{p}$ by a perturbation $\mathbf{h}$ at each iteration[*Gavin*, 2013]. Specifically Levenberg-

169 Marquart was designed to be a sort of meld between two different methods Gradient

170 Decent, and Gauss-Newton. The perturbation vector $\mathbf{h}_{lm}$ can be calculated using the

171 following:

$$\left[\mathbf{J}^T\mathbf{\Sigma}^{-1}\mathbf{J}\right]\mathbf{h}_{lm} = \mathbf{J}^T\mathbf{\Sigma}^{-1}(\mathbf{y} - \boldsymbol{\theta}(\mathbf{p})) \quad (12)$$

172 where $\mathbf{J}$ is the Jacobian matrix $\partial\boldsymbol{\theta}/\partial\mathbf{p}$ [*Levenberg*, 1944; *Marquardt*, 1963].

173   Using the scipy optimize tool box the fitted parameters can determined using the

174 leastsquares function. This function outputs the fitted parameters along with a co-

175 variance matrix. This matrix is calculated using a numerical approximation to the

176 Jacobian matrix that the function uses to determine the solution. The Hessian, $\mathbf{H}$ is

177 then calculated by using the Jacobian and then inverted to get the covariance ma-

trix. Due to the way the numerical routines solve the problem this matrix must be

multiplied by the error between the estimated parameters and the data,

$$\mathbf{\Sigma}_{\hat{\mathbf{p}}} = \frac{(\mathbf{J}^T\mathbf{J})^{-1}(\mathbf{y} - \boldsymbol{\theta}(\hat{\mathbf{p}}))^*\mathbf{\Sigma}^{-1}(\mathbf{y} - \boldsymbol{\theta}(\hat{\mathbf{p}}))}{L - N_{\mathbf{p}}}, \tag{13}$$

where $N_{\mathbf{p}}$ is the number of parameters being fit. The variances of the parameters

are then taken as the diagonals of the matrix. Often though the Hessian matrix is

undefined so it can not be inverted so the error term is then set as a NaN.

4. Simulation Examples

5. Conclusion

Software used to create figures for this publications can be found at

https://github.com/jswoboda/. Please contact the corresponding author, John Swo-

boda at swoboj@bu.edu, with any questions regarding the software along with any

requests for the specific data used for the figures.

References

Butler, T. W., J. Semeter, C. J. Heinselman, and M. J. Nicolls (2010), Imaging f region drifts using monostatic phased-array incoherent scatter radar, *Radio Sci.*, *45*(5), RS5013, doi:10.1029/2010RS004364.

Cohen, L. (1995), *Time Frequency Analysis*, Prentice Hall.

Dahlgren, H., J. L. Semeter, K. Hosokawa, M. J. Nicolls, T. W. Butler, M. G. Johnsen, K. Shiokawa, and C. Heinselman (2012a), Direct three-dimensional imaging of polar ionospheric structures with the resolute bay incoherent scatter radar, *Geophysical Research Letters*, *39*(5), doi:10.1029/2012GL050895.

Dahlgren, H., G. W. Perry, J. L. Semeter, J. P. St. Maurice, K. Hosokawa, M. J. Nicolls, M. Greffen, K. Shiokawa, and C. Heinselman (2012b), Space-time variability of polar cap patches: Direct evidence for internal plasma structuring, *Journal of Geophysical Research: Space Physics*, *117*(A9), doi:10.1029/2012JA017961.

Dougherty, J. P., and D. T. Farley (1960), A theory of incoherent scattering of radio waves by a plasma, *Proceedings of the Royal Society of London. Series A, Mathematical and Physical Sciences*, *259*(1296), pp. 79–99.

Dougherty, J. P., and D. T. Farley (1963), A theory of incoherent scattering of radio waves by a plasma, 3 scattering in a partly ionized gas, *Journal of Geophysical Research*, *68*, 5473.

Farley, D. T. (1969a), Incoherent scatter correlation function measurements, *Radio Sci.*, *4*(10), 935–953.

Farley, D. T. (1969b), Incoherent scatter power measurements; a comparison of various techniques, *Radio Sci.*, *4*(2), 139–142.

Farley, D. T., J. P. Dougherty, and D. W. Barron (1961), A theory of incoherent scattering of radio waves by a plasma ii. scattering in a magnetic field, *Proceedings of the Royal Society of London. Series A, Mathematical and Physical Sciences*, *263*(1313), pp. 238–258.

Gavin, H. P. (2013), The levenberg-marquardt method for nonlinear least squares curve-fitting problems.

Hagfors, T. (1961), Density fluctuations in a plasma in a magnetic field, with applications to the ionosphere, *Journal of Geophysical Research*, *66*(6), 1699–1712, doi:10.1029/JZ066i006p01699.

Hysell, D. L., F. S. Rodrigues, J. L. Chau, and J. D. Huba (2008), Full profile incoherent scatter analysis at jicamarca, *Annales Geophysicae*, *26*(1), 59–75, doi:10.5194/angeo-26-59-2008.

Kay, S. (1993), *Fundamentals of Statistical Signal Processing, Vol. I - Estimation Theory*, Prentice Hall.

Kudeki, E., and M. Milla (2011), Incoherent scatter spectral theories: Part i: A general framework and results for small magnetic aspect angles, *IEEE Transactions on Geoscience and Remote Sensing*, *49*(1), 315–328, doi:10.1109/TGRS.2010.2057252.

Levenberg, K. (1944), A method for the solution of certain non-linear problems in least squares, *Quarterly of Applied Mathematics*, *2*, 164–168.

Marquardt, D. W. (1963), An algorithm for least-squares estimation of nonlinear parmeters, *Journal of the Society for Industrial and Applied Mathematics*, *11*(2), 431–441.

Mitchell, R., and D. Mcpherson (1981), Generating nonstationary random sequences, *Aerospace and Electronic Systems, IEEE Transactions on*, *AES-17*(4), 553–560, doi:10.1109/TAES.1981.309184.

Nicolls, M. J., and C. J. Heinselman (2007), Three-dimensional measurements of traveling ionospheric disturbances with the Poker Flat Incoherent Scatter Radar, *Geophysical Research Letters*.

Nicolls, M. J., R. Cosgrove, and H. Bahcivan (2014), Estimating the vector electric field using monostatic, multibeam incoherent scatter radar measurements, *Radio Science*, *49*(11), 1124–1139, doi:10.1002/2014RS005519.

Nikoukar, R., F. Kamalabadi, E. Kudeki, and M. Sulzer (2008), An efficient near-optimal approach to incoherent scatter radar parameter estimation, *Radio Science*, *43*(5), doi:10.1029/2007RS003724.

Nygren, T. (1996), *Introduction to Incoherent Scatter Measurements*, Invers OY.

Semeter, J., T. Butler, C. Heinselman, M. Nicolls, J. Kelly, and D. Hampton (2009), Volumetric imaging of the auroral ionosphere: Initial results from pfisr, *Journal of Atmospheric and Solar-Terrestrial Physics*, *71*, 738 – 743, doi: 10.1016/j.jastp.2008.08.014.

Shanmugan, K. S., and A. M. Breipohl (1988), *Random Signals Detection Estimation and Data Analysis*, first ed., Wiley.

257 Swoboda, J., J. Semeter, and P. Erickson (2015), Space-time ambiguity functions

258 for electronically scanned isr applications, *Radio Science*, *50*(5), 415–430, doi:
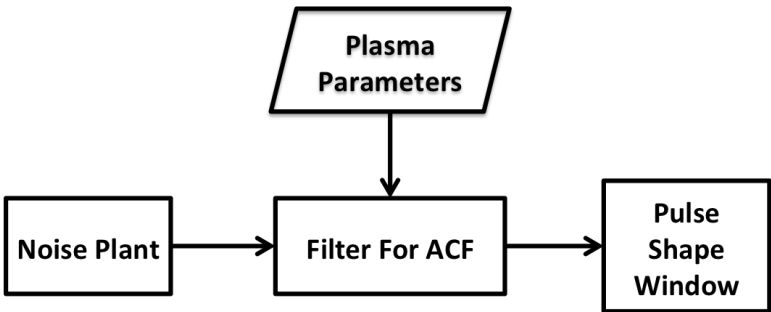
259 10.1002/2014RS005620.

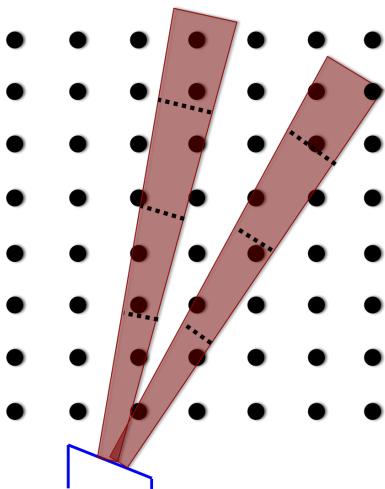**Figure 1.**   Diagram for I/Q simulator signal flow.
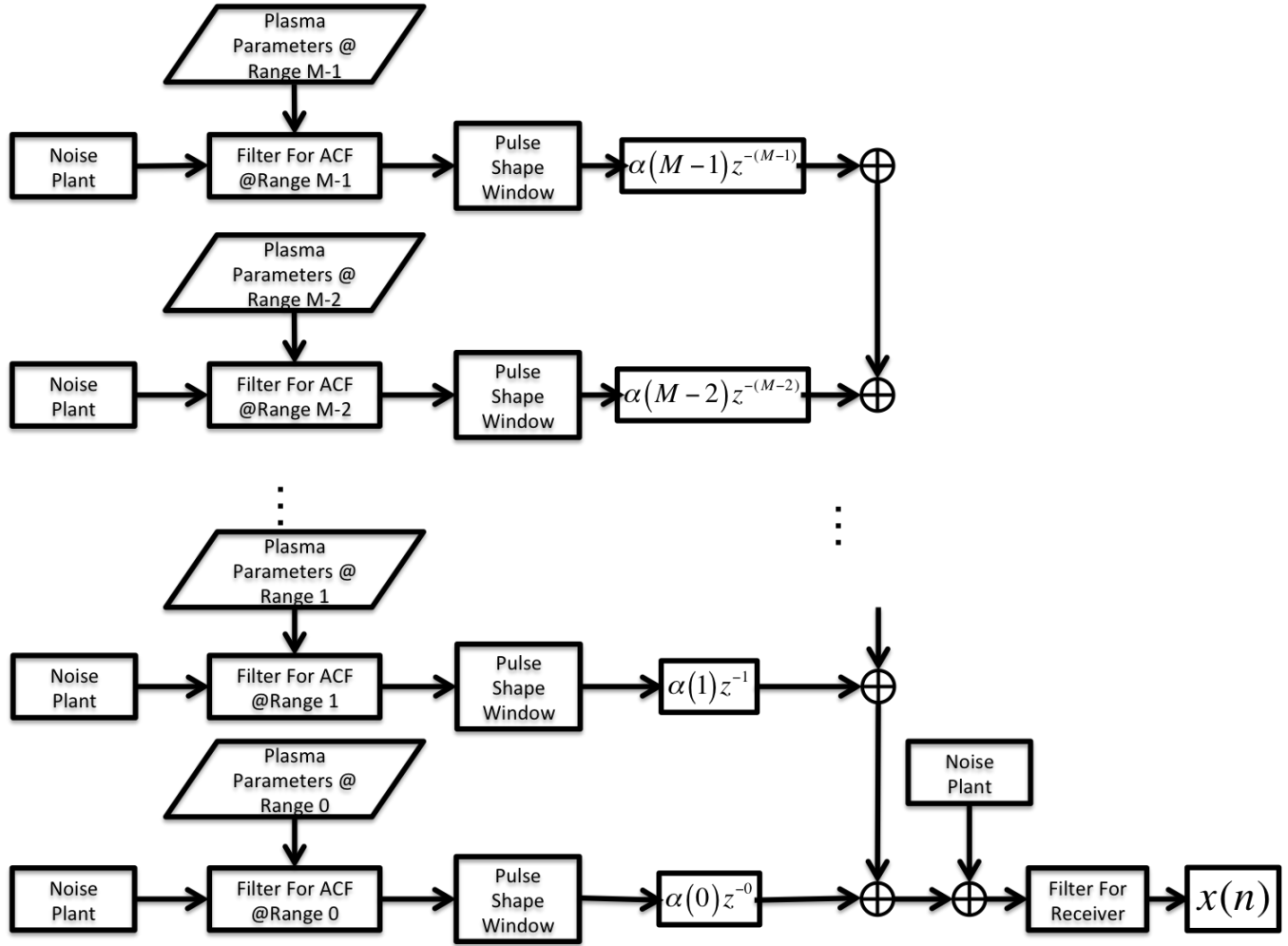

Figure 2.   Beam Sampling Diagram

Figure 3. ISR Simulation Diagram

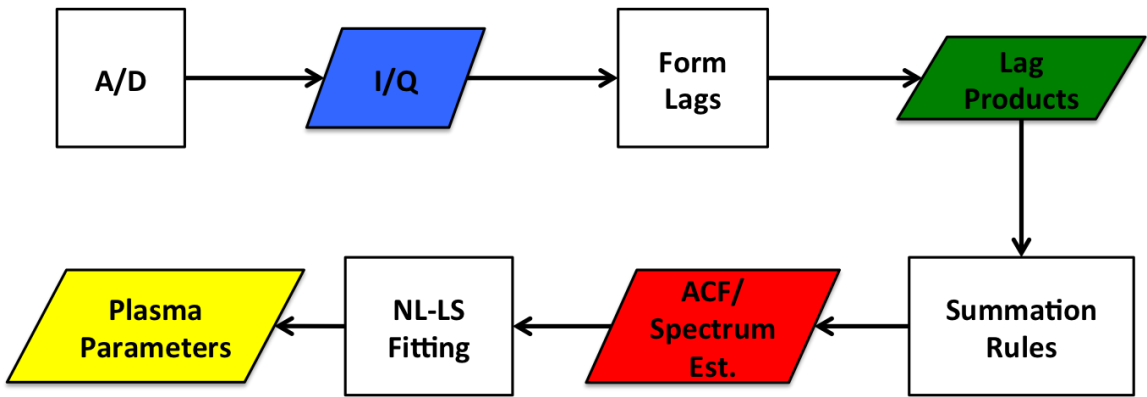**Figure 4.** ISR signal processing chain, with signal processing operations as squares and data products as diamonds.
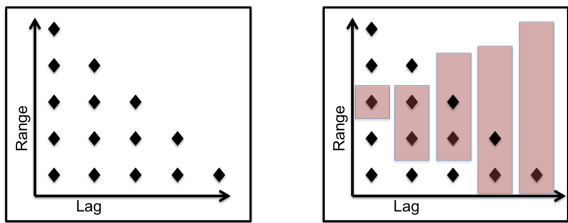

Figure 5. Summation Rule Diagram